

Giant magnetoresistance and topological Hall effect in the EuGa_4 antiferromagnet

H Zhang^{1†}, X Y Zhu^{1†}, Y Xu^{1,*}, D J Gawryluk², W Xie³, S L Ju⁴, M Shi⁴,
T Shiroka^{5,6}, Q F Zhan⁷, E Pomjakushina^{3,*}, and T Shang^{7,*}

¹School of Physics and Electronic Science, East China Normal University, Shanghai 200241, China

²Laboratory for Multiscale Materials Experiments, Paul Scherrer Institut, CH-5232 Villigen PSI, Switzerland

³DESY, Notkestraße 85, D-22607 Hamburg, Germany

⁴Swiss Light Source, Paul Scherrer Institut, CH-5232 Villigen PSI, Switzerland

⁵Laboratory for Muon-Spin Spectroscopy, Paul Scherrer Institut, CH-5232 Villigen PSI, Switzerland

⁶Laboratorium für Festkörperphysik, ETH Zürich, CH-8093 Zurich, Switzerland

⁷Key Laboratory of Polar Materials and Devices (MOE), School of Physics and Electronic Science, East China Normal University, Shanghai 200241, China

E-mail: yxu@phy.ecnu.edu.cn, ekaterina.pomjakushina@psi.ch,
tshang@phy.ecnu.edu.cn

Abstract. We report on systematic temperature- and magnetic field-dependent studies of the EuGa_4 binary compound, which crystallizes in a centrosymmetric tetragonal BaAl_4 -type structure with space group $I4/mmm$. The electronic properties of EuGa_4 single crystals, with an antiferromagnetic (AFM) transition at $T_N \sim 16.4$ K, were characterized via electrical resistivity and magnetization measurements. A giant nonsaturating magnetoresistance was observed at low temperatures, reaching $\sim 7 \times 10^4$ % at 2 K in a magnetic field of 9 T. In the AFM state, EuGa_4 undergoes a series of metamagnetic transitions in an applied magnetic field, clearly manifested in its field-dependent electrical resistivity. Below T_N , in the ~ 4 –7 T field range, we observe also a clear hump-like anomaly in the Hall resistivity which is part of the anomalous Hall resistivity. We attribute such a hump-like feature to the topological Hall effect, usually occurring in noncentrosymmetric materials known to host topological spin textures (as e.g., magnetic skyrmions). Therefore, the family of materials with a tetragonal BaAl_4 -type structure, to which EuGa_4 and EuAl_4 belong, seems to comprise suitable candidates on which one can study the interplay among correlated-electron phenomena (such as charge-density wave or exotic magnetism) with topological spin textures and topologically nontrivial bands.

Keywords: magnetoresistance, topological Hall effect, topological spin textures

Submitted to: *J. Phys.: Condens. Matter*

† These authors contributed equally

1. Introduction

Recently, the study of unconventional Hall effect, including its anomalous-, topological-, and spin-Hall variants, has become one of the preferred methods for investigating the interplay between magnetism and topology in quantum materials [1, 2, 3]. Generally, the Hall effect involves the deflection of charge-carrier trajectories by the Lorentz force. In addition to an external magnetic field (the origin of the classical Hall effect), other sources of the Lorentz force can also be the effective fields associated with a nonzero Berry curvature. To better illustrate this, in general, the Hall resistivity ρ_{xy} can be written as $\rho_{xy} = \rho_{xy}^O + \rho_{xy}^A$, where ρ_{xy}^O and ρ_{xy}^A represent the ordinary- and the anomalous Hall resistivity, respectively. The anomalous Hall effect is usually observed in magnetic materials with a finite magnetization (e.g., ferromagnets or ferrimagnets), which is due to an intrinsic Karplus-Luttinger mechanism, and extrinsic mechanisms like skew scattering and side jump [1]. A finite ρ_{xy}^A due to topologically nontrivial momentum-space features, e.g., Dirac- or Weyl points, currently attracting an intense research interest [4, 5, 6, 7, 8, 9, 10]. For instance, Mn₃Sn, Mn₃Ge, and Mn₃Ir noncollinear antiferromagnets [5, 11, 12, 13], nonmagnetic- TaAs, TaP, and NbP [14, 15] and magnetic- GdPtBi and YbPtBi [9, 16] Weyl semimetals, Cd₃As₂ and ZrTe₅ Dirac semimetals [6, 7, 8], all exhibit ρ_{xy}^A in wide temperature- and magnetic field ranges.

The ρ_{xy}^A term can be further split into two sub-types (owing to their different origins), i.e., $\rho_{xy} = \rho_{xy}^O + \rho_{xy}^{A'} + \rho_{xy}^T$. Here, $\rho_{xy}^{A'}$ represents the conventional anomalous Hall term, mostly determined by the electrical resistivity and magnetization. The second term ρ_{xy}^T indicates a topological Hall term. The topological Hall effect (THE) is considered to be the hallmark of spin textures with a finite scalar spin chirality in real space. Such topological spin textures usually exhibit a nonzero Berry phase, here acting as an effective magnetic field, which gives rise to the topological Hall resistivity ρ_{xy}^T . The THE has been frequently observed in magnetic materials with non-coplanar spin textures, such as skyrmions [3, 17, 18, 19, 20, 21, 22, 23, 24, 25, 26], hedgehogs [27, 28], hopfions [29], merons [30], and magnetic bubbles [31]. Among the notable examples in this regard are the noncentrosymmetric MnSi and analogous compounds [3, 17, 19, 21], where ρ_{xy}^T is caused by magnetic skyrmions.

To date, the topological Hall effect has been studied mostly in transition-metal compounds with a noncentrosymmetric crystal structure [3, 17, 19, 21]. Recently, such studies have been extended to rare-earth magnetic compounds with a centrosymmetric crystal structure [26, 32, 33]. Yet, magnetic materials with a centrosymmetric crystal structure that still can host magnetic skyrmions are rare. In noncentrosymmetric materials, skyrmions can be stabilized by the Dzyaloshinskii-Moriya interaction [34, 35, 36, 37, 38, 39, 40]. Since this is absent in centrosymmetric materials, different mechanisms, including magnetic frustration and fluctuation or the competition between magnetic interactions and magnetic anisotropies, have been proposed to lead to the formation of skyrmions [26, 32, 33, 41, 42, 43]. Nevertheless, such mechanisms cannot account for all the cases where skyrmions are observed in centrosymmetric materials. Hence, their

origin is not yet fully understood and requires further investigations.

The discovery of nontrivial band topology and large magnetoresistance (MR) in the prototype compound BaAl₄ has stimulated considerable interest in this family of materials [44]. Similar to BaAl₄, also BaGa₄ exhibits metallic behavior without undergoing any phase transitions, while SrAl₄ shows a charge-density-wave (CDW) and a structural phase transition at $T_{\text{CDW}} \sim 250$ K and $T_{\text{S}} \sim 90$ K, respectively [45]. Both compounds are also expected to exhibit topological features. Unlike these nonmagnetic materials, upon replacing Ba (or Sr) with Eu, the 4*f* electrons bring new intriguing aspects to the topology, as clearly illustrated by our recent work on EuAl₄ [46]. EuAl₄ exhibits coexisting antiferromagnetic- (AFM) and CDW orders with onset temperatures of $T_{\text{N}} \sim 15.6$ K and $T_{\text{CDW}} \sim 140$ K [46, 47, 48, 49, 50, 51] and undergoes a series of metamagnetic transitions in the AFM state [46, 49]. Within the ~ 1 – 2.5 T field range, a clear hump-like anomaly was observed in the Hall resistivity, most likely a manifestation of THE [46]. Hence, EuAl₄ represents a rare case where the topological Hall effect not only arises in a centrosymmetric structure, but it also coexists with CDW order.

EuGa₄ is also an antiferromagnet (with $T_{\text{N}} \sim 16.5$ K), whose CDW order starts to emerge under applied pressure close to 0.75 GPa, with T_{CDW} reaching ~ 175 K at 2.3 GPa [49, 52]. Although EuAl₄ and EuGa₄ share similar magnetic properties, much less is known about EuGa₄, in particular, with regard to its topological transport properties. Most of the previous work on EuGa₄ has focused on its temperature-dependent aspects, while its electrical transport properties under applied magnetic field have been somewhat overlooked [51, 52]. Here, by investigating the temperature- and field-dependent electrical resistivity and magnetization of EuGa₄, we report the observation of (i) a giant nonsaturating MR, whose origin is most likely attributed to a nontrivial band structure; (ii) a hump-like anomaly in the Hall resistivity, most likely attributed to the topological Hall effect induced by topological spin textures.

2. Experimental details

Single crystals of EuGa₄ were grown by a molten Ga flux method. High purity Eu rods (Alfa Aesar, 99.9%) and Ga ingots (Alfa Aesar, 99.999%) in a ratio of 1:9 were loaded in an alumina crucible and sealed in a quartz ampule. Then, the quartz ampule was heated up to 750°C at a rate of 200°C/h. After annealing at this temperature for more than 10 h, the ampule was slowly cooled down to 400°C at a rate of 1°C/h. After removing the excess Ga flux using a centrifuge, centimetre-sized single crystals were obtained [see example in the inset of figure 1(b)].

The phase purity and the orientation of EuGa₄ crystals were checked by x-ray diffraction (XRD) measurements using a Bruker D8 diffractometer. The electrical resistivity and magnetization were measured in a Quantum Design MPMS and PPMS on oriented single crystals with typical dimension of $3 \times 1 \times 0.25$ mm³, respectively. For the magnetization measurements, the magnetic field was applied along the *c*-axis. For the resistivity measurements, the electric current (5 mA) was applied in the *ab*-plane, while

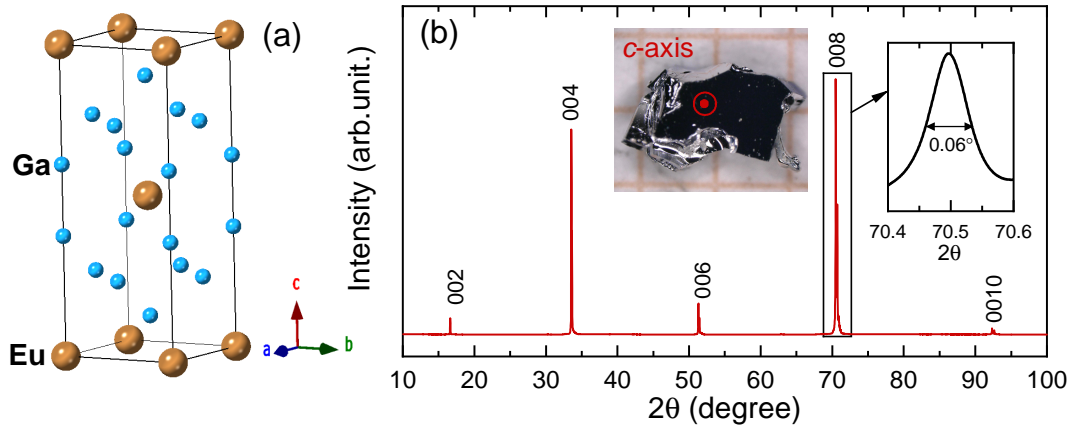


Figure 1. (a) Crystal structure of EuGa_4 . (b) XRD pattern of an EuGa_4 single crystal. The inset in (b) shows a picture of the crystal, whose c -axis is normal to the plane. The rather narrow (008) reflection, shown enlarged in the inset, indicates a good sample quality.

the magnetic field was applied along the c -axis. The field-dependent electrical resistivity was investigated using both positive and negative magnetic fields. To avoid spurious resistivity contributions due to misaligned Hall probes, the longitudinal contribution to the Hall resistivity ρ_{xy} , was removed by an anti-symmetrization procedure, i.e., $\rho_{xy}(H) = [\rho_{xy}(H) - \rho_{xy}(-H)]/2$. Similarly, in case of longitudinal electrical resistivity ρ_{xx} measurements, the spurious transverse contribution was removed by a symmetrization procedure, i.e., $\rho_{xx}(H) = [\rho_{xx}(H) + \rho_{xx}(-H)]/2$.

3. Results and discussion

Figure 1(a) shows the crystal structure of EuGa_4 , where three Ga- and one Eu-layers stack alternatively along the c -axis. No foreign phases could be identified in the powder XRD pattern, thus indicating that the obtained EuGa_4 crystals are in a pure phase. The XRD pattern is well indexed by a tetragonal crystal structure with space group $I4/mmm$ (No. 139), fairly typical of many binary- and ternary derivative compounds [53], as e.g., iron-based superconductors and heavy-fermion compounds. The crystal orientation was determined from XRD patterns of EuGa_4 single crystals. As shown in figure 1(b), only (00 l) reflections could be detected for the crystal depicted in the inset, thus implying that its c -axis is perpendicular to the EuGa_4 crystal plane. The good quality of EuGa_4 crystals was also confirmed by a relatively small full width at half maximum (FWHM), here $\sim 0.06^\circ$ for the (008)-reflection, as shown in the inset of figure 1(b).

Figure 2(a) presents the temperature dependence of the dc magnetic susceptibility $\chi(T)$ of EuGa_4 between 2 to 300 K, measured in a field of $\mu_0 H = 0.1$ T, applied both parallel (χ_c) and perpendicular (χ_{ab}) to the c -axis. For both orientations, as indicated by the arrow in figure 2(a), the magnetic susceptibility exhibits a clear anomaly around $T_N \sim 16.4$ K, which corresponds to the AFM transition of Eu $4f$ electrons. The zero-field-cooling- and field-cooling magnetic susceptibilities are practically identical, confirming the AFM nature

Giant MR and THE in the EuGa_4 antiferromagnet

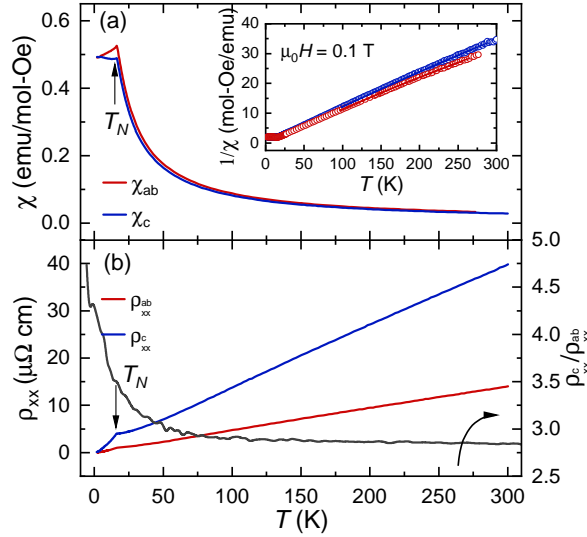


Figure 2. Temperature dependence of the magnetic susceptibility (a) and electrical resistivity (b) for EuGa_4 . The inset shows the inverse magnetic susceptibility $1/\chi$ vs. temperature, where the solid lines are fits to the Curie-Weiss model. The arrows indicate an antiferromagnetic transition at $T_N \sim 16.3$ K. The magnetic susceptibility was measured by applying a magnetic field $\mu_0 H = 0.1$ T, both parallel (χ_c) and perpendicular (χ_{ab}) to the c -axis. The electrical resistivity was measured in zero field with the current applied both parallel (ρ_{xx}^c) and perpendicular (ρ_{xx}^{ab}) to the c -axis. The ratio of $\rho_{xx}^c/\rho_{xx}^{ab}$ is also shown in (b) (right-axis).

of the magnetic transition. Both χ_c and χ_{ab} are comparable in the AFM state and are almost identical in the paramagnetic (PM) state, indicating the lack of a strong magnetic anisotropy in EuGa_4 . The magnetic susceptibility in the PM state can be described by the modified Curie–Weiss model, $\chi(T) = \chi_0 + C/(T - \theta_p)$, with χ_0 being a temperature independent susceptibility, including contributions from the core diamagnetism, the van Vleck paramagnetism, and the Pauli paramagnetism; C is the Curie constant and θ_p the PM Curie temperature. The inset of figure 2(a) shows the inverse susceptibility $1/\chi(T)$ versus T for both χ_c and χ_{ab} , respectively, with the solid lines being fits to the Curie–Weiss model over the temperature range 150–300 K. The slope of the fits, allows the determination of the effective magnetic moment μ_{eff} from the Curie constant. For χ_c , the $\mu_{\text{eff}} = 7.90(5) \mu_B$, $\chi_0 = 2.6(2) \times 10^{-3}$ emu/mol-Oe, and $\theta_p = 2(1)$ K; while for χ_{ab} , the $\mu_{\text{eff}} = 7.95(5) \mu_B$, $\chi_0 = 4.7(3) \times 10^{-3}$ emu/mol-Oe, and $\theta_p = 5(1)$ K. For both orientations, the effective moments are comparable to the theoretical value for free Eu^{2+} ions ($7.94 \mu_B$).

The temperature-dependent zero-field electrical resistivity, $\rho_{xx}(T)$, measured between 2 and 300 K, with the electric current applied either parallel (ρ_{xx}^c) or perpendicular (ρ_{xx}^{ab}) to the c -axis, is shown in figure 2(b). EuGa_4 demonstrates a fairly good metallic behavior. The conspicuous difference between ρ_{xx}^c and ρ_{xx}^{ab} persists down to the lowest temperature, with the ratio $\rho_{xx}^c/\rho_{xx}^{ab}$ reaching ~ 5 at 2 K, and is consistent with previous studies [52]. Such highly anisotropic transport properties are most likely attributed to an elongated Fermi surface along the c -axis [51, 52] or to a different carrier mobility, the latter having been proved by Hall measurements in the sister compound EuAl_4 [47]. At low

Giant MR and THE in the EuGa_4 antiferromagnet

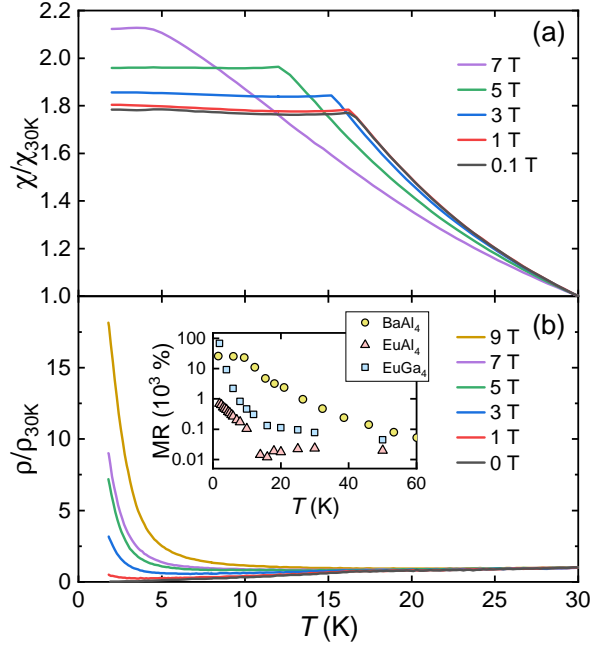


Figure 3. Temperature dependence of the magnetic susceptibility $\chi(T, H)$ (a) and electrical resistivity $\rho_{xx}(T, H)$ (b) for EuGa_4 , measured in various magnetic fields up to 9 T. Here, the magnetic fields are applied along the c -axis. Both the $\chi(T, H)$ and $\rho_{xx}(T, H)$ datasets are normalized to the respective 30-K values. The inset summarizes the magnetoresistance of EuAl_4 , EuGa_4 , and of their nonmagnetic counterpart BaAl_4 below 60 K in a field of 9 T. The magnetoresistance is defined as $\text{MR} = [\rho_{xx}(9\text{T}) - \rho_{xx}(0\text{T})] / \rho_{xx}(0\text{T})$. Note the logarithmic scale. The data of BaAl_4 and EuAl_4 were taken from Ref. [44, 46].

temperatures, due to a reduced magnetic scattering, both ρ_{xx}^c and ρ_{xx}^{ab} exhibit a sudden decrease, signaling the onset of an AFM transition of the Eu $4f$ electrons. As indicated by the arrow in figure 2(b), the T_N determined from electrical resistivity is consistent with that from magnetic susceptibility.

To further investigate the magnetic and transport properties of EuGa_4 , both the temperature-dependent magnetic susceptibility $\chi(T, H)$ and electrical resistivity $\rho_{xx}(T, H)$ were measured under various magnetic fields up to 9 T. Unlike EuAl_4 , whose magnetic susceptibility exhibits four successive AFM transitions, only one AFM transition can be identified in the $\chi(T)$ data of EuGa_4 . As can be seen in figure 3(a), upon increasing the magnetic field, the AFM transition is progressively suppressed towards lower temperatures, reaching $T_N \sim 4.2$ K at 7 T. As for $\rho_{xx}(T, H)$ in figure 3(b), the AFM transition can still be identified for applied magnetic fields below 5 T [see also zero-field resistivity in figure 2(b)], yet it becomes less visible in magnetic fields above 5 T, because of the onset of a giant MR at low temperatures. Below 20 K, the magnetoresistance of EuGa_4 increases exponentially, reaching almost $\sim 7 \times 10^4$ % at 2 K, a record among the materials belonging to the BaAl_4 -type family. The MRs vs. temperature of EuAl_4 , EuGa_4 , and of their nonmagnetic counterpart BaAl_4 are summarized in the inset of figure 3(b). Neither EuAl_4 , nor EuGa_4 exhibits clear anomalies at the respective AFM transitions. Considering that the nonmagnetic BaAl_4 also shows a giant MR at low temperatures [44], we believe that the magnetic order of Eu^{2+}

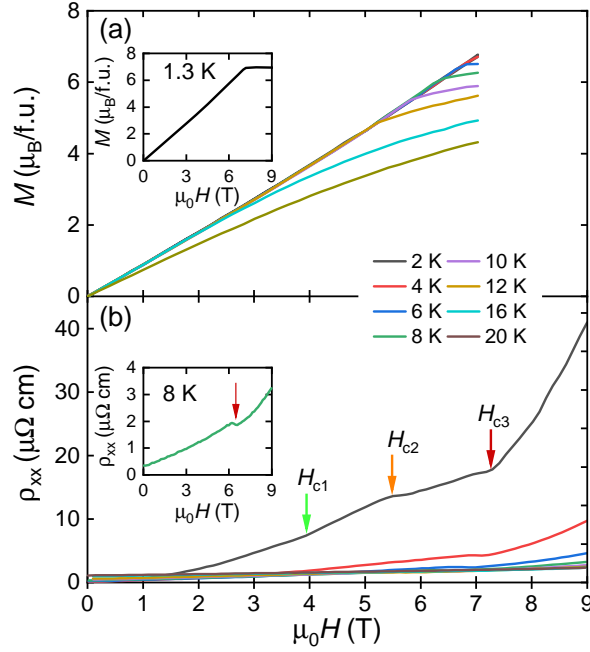


Figure 4. Magnetic field dependence of the magnetization $M(H, T)$ (a) and electrical resistivity $\rho_{xx}(H, T)$ (b) for EuGa_4 , collected at various temperatures. The magnetic field was applied along the c -axis. The arrows in (b) mark the transitions at H_{c1} , H_{c2} , and H_{c3} , respectively. The inset in panel (a) shows $M(H)$ at 1.3 K, with the data taken from Ref. [52]. Inset in (b) shows $\rho_{xx}(H)$ at 8 K, where only one transition can be identified.

ions shows weak correlation to the appearance of such a giant nonsaturating MR in EuAl_4 and EuGa_4 . Most likely their prominent MR can be attributed to a modification of the Fermi surface topology by the applied magnetic field, similar to that observed in other topological materials [54, 55].

Figure 4 reports the field dependence of magnetization $M(H, T)$ and electrical resistivity $\rho_{xx}(H, T)$ of EuGa_4 at various temperatures, covering both the AFM and PM states, with the magnetic field applied along the c -axis. As shown in the inset of figure 4(a), $M(H)$ at 1.3 K starts to saturate for magnetic fields above ~ 7.2 T, i.e., slightly above the highest field we could apply in this study. For both field orientations, the saturation magnetization $M_s \sim 6.9 \mu_B$ is consistent with $7.0 \mu_B$, the expected value for the $J = 7/2$ Eu^{2+} ions [52]. Such saturation field decreases as the temperature increases, reaching ~ 5.3 T at 12 K. The sublinear $M(H)$ in the PM states suggests the presence of magnetic fluctuations near the AFM order, as have been observed also in EuAl_4 [46]. Unlike the EuAl_4 case, whose magnetization shows three metamagnetic transitions, accompanied by a small yet clear hysteresis in the AFM state, the magnetization of EuGa_4 shows only a smooth saturation, independent of the direction of the applied magnetic field. Surprisingly, when measuring the field-dependent electrical resistivity, one can still identify three distinct transitions in the AFM state. For example, as shown in figure 4(b), $\rho_{xx}(H, 2\text{K})$ undergoes three transitions at $\mu_0 H_{c1} \sim 3.8$ T, $\mu_0 H_{c2} \sim 5.6$ T, and $\mu_0 H_{c3} \sim 7.1$ T, respectively, which can be clearly tracked also in the first derivative of ρ_{xx} with respect to the magnetic field. The critical fields H_{c3} are consistent with the saturation fields determined from the $M(H)$.

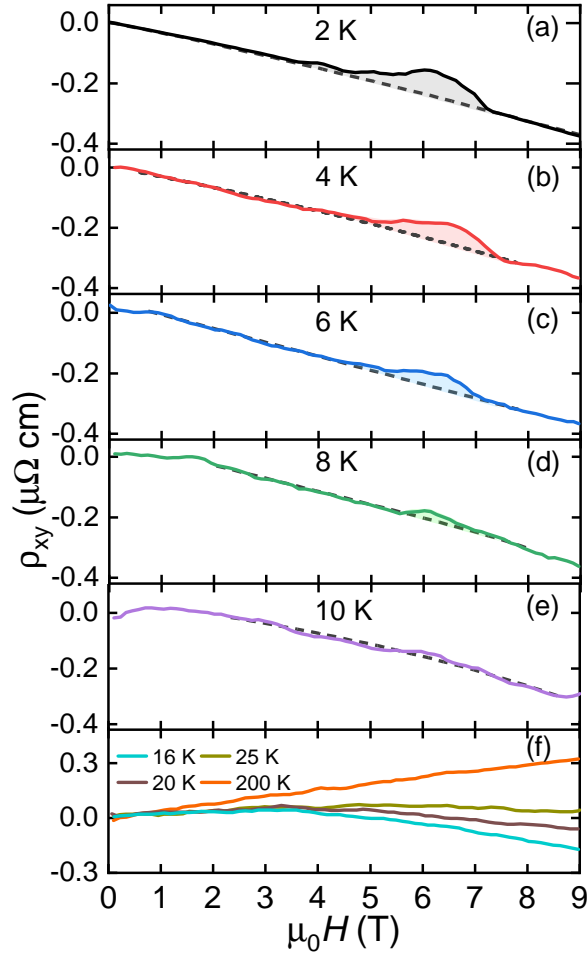


Figure 5. Magnetic field dependence of the Hall resistivity $\rho_{xy}(H, T)$ of EuGa_4 , collected at various temperatures, covering both the AFM and PM states. The magnetic field was applied along the c -axis. The dashed lines in (a)-(e) represent polynomial fits.

The transitions at H_{c1} and H_{c2} are most likely two metamagnetic transitions, similar to those observed also in EuAl_4 . Why such metamagnetic transitions do not show up in the magnetization data requires further investigation. Upon increasing the temperature, H_{c2} remains almost constant and it disappears for $T > 4.5$ K. At the same time, H_{c1} increases slowly with temperature, reaching 4.8 T at 7 K. Above 7 K, only one transition can be identified in the $\rho_{xx}(H)$ data, as indicated by the arrow in the inset of figure 4(b). The H_{c3} values determined from electrical-resistivity data are highly consistent with those from magnetization results, as well as with those of previous studies (see magnetic phase diagram below) [52]. Note that, both transitions at H_{c1} and H_{c2} are essentially not reported in previous studies [52].

The field-dependent Hall resistivity $\rho_{xy}(H)$ collected at various temperatures are presented in figure 5. In the PM state, as the temperature decreases, the slope of $\rho_{xy}(H)$ changes from positive to negative, implying that EuGa_4 , too, is a multiband system. The multiband nature of EuGa_4 is clearly evident from the nonlinear behavior of $\rho_{xy}(H)$ [see e.g., $\rho_{xy}(H)$ at 20 K in figure 5(f)], as confirmed also by de Haas–van Alphen (dHvA)

studies and by electronic band-structure calculations [48, 49, 52]. Similar to BaAl₄ and EuAl₄ [44, 46, 47], at high temperatures, the $\rho_{xy}(H)$ of EuGa₄ is dominated by the holes while, at low temperatures, mostly the electrons account for the Hall signal. In the AFM state [see figures 5(a)-(d)], a hump-like anomaly in the $\rho_{xy}(H)$ gradually develops with decreasing temperature, reminiscent of the topological Hall resistivity arising from topological spin textures [3, 17, 19, 21, 23, 24, 25, 26, 27, 28, 29, 31]. Such anomaly is clearly evident at low temperatures, but it almost disappears at temperatures above 10 K [see figure 5(e)]. To determine unambiguously the topological contribution ρ_{xy}^T , the ordinary (ρ_{xy}^O) and the conventional anomalous (ρ_{xy}^A) contributions have to be subtracted from the measured ρ_{xy} . In the EuGa₄ case, its multiband nature makes the subtraction of ρ_{xy}^O unreliable. Since the hump-like Hall resistivity feature appears only in a narrow field range, to extract this anomaly from the $\rho_{xy}(H)$ data, we chose to subtract a polynomial background [see the dotted lines in figures 5(a)-(d)]. Note that $\Delta\rho_{xy}$ is part of the anomalous Hall resistivity, i.e., it might be either trivial (conventional anomalous Hall resistivity ρ_{xy}^A) or nontrivial (topological Hall resistivity ρ_{xy}^T). The subtracted $\Delta\rho_{xy}(H)$ of EuGa₄ are plotted in figure 6, together with its magnetic phase diagram. Independent of its nature, clearly $\Delta\rho_{xy}$ is most prominent in the AFM state, at temperatures below 10 K and in a field range between H_{c1} and H_{c3} , with 10 K representing the critical temperature below which H_{c1} sets in.

First, we discuss the giant and nonsaturating positive magnetoresistance of EuGa₄. Large nonsaturating MR seems increasingly ubiquitous in semimetals [6, 54, 56, 57, 58]. The two most frequently discussed scenarios for explaining the large MR of semimetals are: (i) the charge compensation in a semiclassical two-carrier model and (ii) the guiding center motion of charge carriers. The latter is usually relevant for topological semimetals with a linear dispersion (see e.g., Ref [59]). In the nonmagnetic BaAl₄, the charge compensation is not yet achieved and its large nonsaturating MR is associated with the Dirac spectrum [44]. EuGa₄ exhibits comparable MR to the BaAl₄, reaching $\sim 7 \times 10^4\%$ [see details in the inset of figure 3(b)]. Previous dHvA studies and electronic band structure calculations proposed that the charge compensation might be achieved in the PM state of EuGa₄ [52]. In the AFM state, the MR increases exponentially, making the estimation of the carrier type and density from the Hall resistivity of a two-band model unreliable. Although a possibility of charge compensation cannot be fully excluded, the comparison with BaAl₄ suggests a topological nontrivial origin of the giant and nonsaturating MR in EuGa₄. Furthermore, in most of the nonmagnetic semimetals, apart from quantum oscillations, the MR exhibits a linear ($\sim H$) or a quadratic ($\sim H^2$) magnetic field dependence. Obviously, the anomalies at the three critical fields in the MR of EuGa₄ are not related to quantum oscillations [see figure 4(b)]. Considering that a finite $\Delta\rho_{xy}$ —possibly signaling topological spin textures—appears mostly in the field range between H_{c1} and H_{c3} [see figure 6(b)], the anomalies at H_{c1} and H_{c2} are expected to be metamagnetic transitions. At the same time, the critical field H_{c3} is consistent with the saturation field in the magnetization data. Such metamagnetic transitions might be related to a subtle change of spin direction or magnetic vectors, but their absence in the magnetization data is puzzling and requires further investigation.

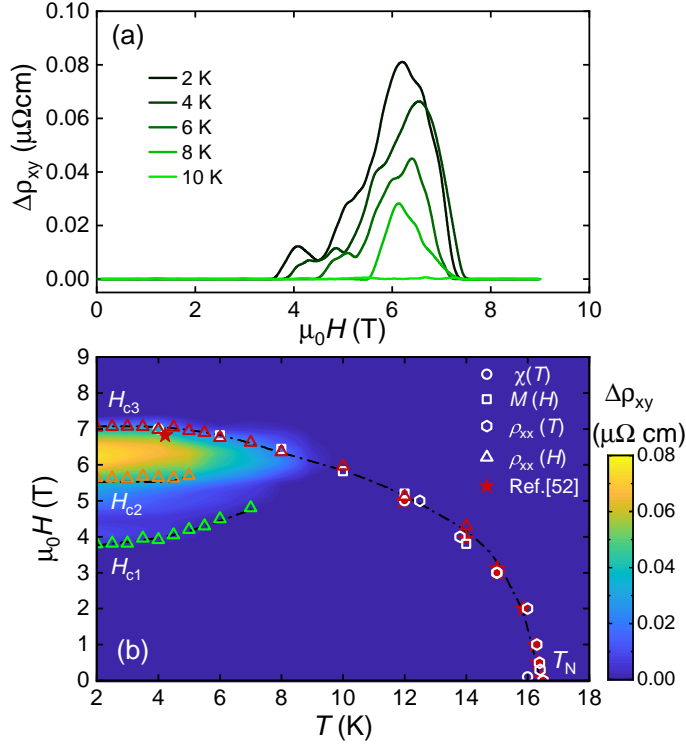


Figure 6. (a) Field dependence of the extracted Hall resistivity $\Delta\rho_{xy}$ of EuGa_4 at various temperatures (see text for the definition of $\Delta\rho_{xy}$). (b) Magnetic phase diagram of EuGa_4 , with the field applied along the c -axis. The critical temperatures are determined from $\chi(T)$ and $\rho_{xx}(T)$ under various magnetic fields, while the critical fields are determined from $M(H)$ and $\rho_{xx}(H)$ at various temperatures. The background color in (b) represents the magnitude of $\Delta\rho_{xy}(H)$ at various temperatures. Dash-dotted lines are guides to the eyes. Data taken from Ref. [52] (here shown with stars) are highly consistent with our results.

A combination of charge compensation, nontrivial band topology, and topological spin textures, may lead to these interesting features in the magnetoresistance of EuGa_4 .

Now we discuss the origin of the hump-like anomaly in $\rho_{xy}(H)$. To check whether a nonzero topological Hall resistivity ρ_{xy}^T underlies the hump-like anomaly in $\rho_{xy}(H)$, a knowledge of the exact field evolution of the ordinary $\rho_{xy}^O(H)$ - and conventional anomalous $\rho_{xy}^{A'}(H)$ Hall contributions is crucial. As discussed above, $\rho_{xy}^O(H)$ is unknown a priori, but it is presumably a nonlinear function of field due to the multiband nature of EuGa_4 . Furthermore, the extraction of conventional anomalous Hall resistivity $\rho_{xy}^{A'}$ is even more complex in EuGa_4 . Conventionally, $\rho_{xy}^{A'}$ can be rewritten as $R_s M$, $S_H \rho_{xx}^2 M$, or $S'_H \rho_{xx} M$, where R_s , S_H and S'_H are constants, and M and ρ_{xx} are the field-dependent magnetization and electrical resistivity, respectively. In real materials, $\rho_{xy}^{A'}$ depends on the mechanisms of intrinsic-, side-jump-, skew scattering-, or an intricate combination thereof [60, 61, 62]. These different representations together with the multiband nature of EuGa_4 make the extraction of ρ_{xy}^T from the measured ρ_{xy} even more complicated, especially considering the presence of a giant MR in the AFM state of EuGa_4 . Different methods have been employed to evaluate $\rho_{xy}^{A'}(H)$ in EuAl_4 , leading to different explanations for the hump-like anomaly

in $\rho_{xy}(H)$. Consequently, the observed $\Delta\rho_{xy}$ in figure 6(a) may correspond exactly to a topological Hall term ρ_{xy}^T , or to the lower/upper limits of ρ_{xy}^T [46]. For EuGa₄, although a quantitative extraction of ρ_{xy}^T is not yet feasible, it seems that the hump-like anomaly between H_{c1} and H_{c3} cannot be reproduced either by a multi-band $\rho_{xy}^O(H)$ (which should evolve smoothly with magnetic field), or by a ρ_{xy}^A in the form of $R_s M$, $S_H \rho_{xx}^2 M$, or $S'_H \rho_{xx} M$. Therefore, a nonzero ρ_{xy}^T , closely related to the topological spin textures, should be present in EuGa₄. To confirm such topological magnetic phase in EuGa₄, further experiments, as e.g., resonant x-ray scattering or Lorentz transmission electron microscopy, are highly desirable.

The observation of a topological Hall effect in magnetic materials is usually attributed to noncoplanar spin textures, such as magnetic skyrmions, characterized by a finite scalar spin chirality in real space. Magnetic skyrmions can be stabilized by the Dzyaloshinskii-Moriya interaction and, thus, are often observed in noncentrosymmetric magnetic materials and magnetic thin films [34, 35, 36, 37, 38, 39, 40]. Alternatively, skyrmions can be also stabilized by magnetic frustrations and fluctuations or by the competition between the magnetic interactions and magnetic anisotropies in centrosymmetric systems, where the Dzyaloshinskii-Moriya interaction cannot exist [26, 32, 33, 41, 42, 43]. Skyrmions in centrosymmetric materials exhibit the unique advantage of a tunable skyrmion size and spin helicity and are hence intensively pursued [63]. However, to date, only a few centrosymmetric systems have been found to host skyrmions, e.g., Gd₂PdSi₃ [26], Gd₃Ru₄Al₁₂ [32], GdRu₂Si₂ [33], Fe₃Sn₂ [43], and, possibly, also EuCd₂As₂ and EuAl₄ [10, 46]. The observation of a topological Hall effect in EuGa₄ not only adds another rare-earth-based skyrmion material, but might also provides clues to the tuning of topological spin textures and other ordered states. For EuAl₄, the THE appears in a field range of 1 to 2 T [46]. While in EuGa₄, as shown in figure 6(b), the THE shows up between 4 and 7 T. Therefore, the critical field to induce the THE in EuAl₄ is about 3 times smaller than in EuGa₄. On the other hand, a CDW order sets in at $T_{CDW} \sim 140$ K at ambient pressure in EuAl₄ [46, 47, 48, 49, 50, 51], whereas physical- or chemical pressure is necessary to induce the CDW order in EuGa₄ [49, 52, 64]. The T_{CDW} decreases with increasing pressure in EuAl₄, while it does exactly the opposite in EuGa₄ [49, 52]. At low temperatures, in both EuAl₄ and EuGa₄, T_N increases with increasing pressure, exceeding 30 K at a pressure of 5 GPa in EuAl₄ [49, 52]. Future studies on the evolution of ρ_{xy}^T with pressure in Eu(Ga_{1-x}Al_x)₄ could shed light on the exotic magnetic phase with topological spin textures of such systems.

In addition to the topological spin textures, upon breaking certain symmetries, noncollinear antiferromagnets may also exhibit a topological Hall effect due to Berry curvature, such as at the Dirac or Weyl points [65]. Such a momentum-space scenario has been theoretically proposed and experimentally observed, for instance, in Mn₃(Sn,Ge) [5, 13, 11] and (Yb,Gd)PtBi [9, 16]. A three-dimensional Dirac spectrum with nontrivial topology and possible nodal-lines crossing the Brillouin zone has been recently observed in nonmagnetic BaAl₄ [44]. The giant nonsaturating MR in EuGa₄ hints at the existence of a topologically nontrivial band structure, which may cooperate with topological spin

textures and, thus, contribute to the topological Hall effect.

4. Summary

To summarize, we observed a giant nonsaturating magnetoresistance and a hump-like anomaly $\Delta\rho_{xy}$ in the Hall resistivity of the centrosymmetric antiferromagnet EuGa₄. Analogous to the nonmagnetic BaAl₄, the MR of EuGa₄ could originate from its nontrivial band topology. By systematic temperature- and field-dependent electrical resistivity and magnetization measurements, we could establish the magnetic phase diagram of EuGa₄. Similarly to EuAl₄, the hump-like anomaly in the Hall resistivity of EuGa₄ appears mostly in a field range where also metamagnetic transitions occur. Such hump-like anomaly is most likely an indication of the topological Hall effect. Although a trivial origin of the effect cannot be fully excluded, our results suggest that a topological Hall effect and topological spin textures, such as magnetic skyrmions, may indeed exist in EuGa₄. Therefore, the material family with a tetragonal BaAl₄-type structure, to which EuGa₄ and EuAl₄ belong, seems to comprise suitable candidates on which one can study the interplay between correlated-electron phenomena (such as charge-density wave or exotic magnetism) with topological spin textures and topologically nontrivial band structures.

5. Acknowledgements

T.S. acknowledges support from the Natural Science Foundation of Shanghai (Grant Nos. 21ZR1420500 and 21JC1402300) and the Schweizerische Nationalfonds zur Förderung der Wissenschaftlichen Forschung (SNF) (Grant Nos. 200021_188706 and 206021_139082). Y.X. acknowledges support from the Shanghai Pujiang Program (Grant No. 21PJ1403100). This work was also financially supported by the National Natural Science foundation of China (NSFC) (Grant Nos. 12174103 and 11874150) and the Sino-Swiss Science and Technology Cooperation (Grant No. IZLCZ2-170075).

6. References

- [1] Nagaosa N, Sinova J, Onoda S, MacDonald A H and Ong N P 2010 *Rev. Mod. Phys.* **82** 1539
- [2] Sinova J, Valenzuela S O, Wunderlich J, Back C H and Jungwirth T 2015 *Rev. Mod. Phys.* **87** 1213
- [3] Neubauer A, Pfleiderer C, Binz B, Rosch A, Ritz R, Niklowitz P G and Böni P 2009 *Phys. Rev. Lett.* **102** 186602
- [4] Onoda M, Tatara G and Nagaosa N 2004 *J. Phys. Soc. Jpn.* **73** 2624
- [5] Nakatsuji S, Kiyohara N and Higo T 2015 *Nature* **527** 212
- [6] Liang T, Gibson Q, Ali M N, Liu M, Cava R J and Ong N P 2015 *Nat. Mater.* **14** 280
- [7] Liang T, Lin J, Gibson Q, Gao T, Hirschberger M, Liu M, Cava R J and Ong N P 2017 *Phys. Rev. Lett.* **118** 136601
- [8] Liang T, Lin J, Gibson Q, Kushwaha S, Liu M, Wang W, Xiong H, Sobota J A, Hashimoto M, Kirchmann P S, Shen Z X, Cava R J and Ong N P 2018 *Nat. Phys.* **14** 451
- [9] Suzuki T, Chisnell R, Devarakonda A, Liu Y T, Feng W, Xiao D, Lynn J W and Checkelsky J G 2016 *Nat. Phys.* **12** 1119

Giant MR and THE in the EuGa_4 antiferromagnet

- [10] Xu Y, Das L, Ma J Z, Yi C J, Nie S M, Shi Y G, Tiwari A, Tsirkin S S, Neupert T, Medarde M, Shi M, Chang J and Shang T 2021 *Phys. Rev. Lett.* **126** 076602
- [11] Ikhlas M, Tomita T, Koretsune T, Suzuki M T, Nishio-Hamane D, Arita R, Otani Y and Nakatsuji S 2017 *Nat. Phys.* **13** 1085
- [12] Chen H, Niu Q and MacDonald A 2014 *Phys. Rev. Lett.* **112** 017205
- [13] Nayak A K, Fischer J E, Sun Y, Yan B, Karel J, Komarek A C, Shekhar C, Kumar N, Schnelle W, Kübler J, Felser C and Parkin S S P 2016 *Sci. Adv.* **2** e1501870
- [14] Cagliaris F, Wuttke C, Sykora S, Süß V, Shekhar C, Felser C, Büchner B and Hess C 2018 *Phys. Rev. B* **98** 201107(R)
- [15] Watzman S J, McCormick T M, Shekhar C, Wu S C, Sun Y, Prakash A, Felser C, Trivedi N and Heremans J P 2018 *Phys. Rev. B* **97** 161404(R)
- [16] Guo C Y, Wu F, Wu Z Z, Smidman M, Cao C, Bostwick A, Jozwiak C, Rotenberg E, Liu Y, Steglich F and Yuan H Q 2018 *Nat. Commun.* **9** 4622
- [17] Gayles J, Freimuth F, Schena T, Lani G, Mavropoulos P, Duine R A, Blügel S, Sinova J and Mokrousov Y 2015 *Phys. Rev. Lett.* **115** 036602
- [18] Lee M, Kang W, Onose Y, Tokura Y and Ong N P 2009 *Phys. Rev. Lett.* **102** 186601
- [19] Kanazawa N, Onose Y, Arima T, Okuyama D, Ohoyama K, Wakimoto S, Kakurai K, Ishiwata S and Tokura Y 2011 *Phys. Rev. Lett.* **106** 156603
- [20] Li Y, Kanazawa N, Yu X Z, Tsukazaki A, Kawasaki M, Ichikawa M, Jin X F, Kagawa F and Tokura Y 2013 *Phys. Rev. Lett.* **110** 117202
- [21] Franz C, Freimuth F, Bauer A, Ritz R, Schnarr C, Duvinage C, Adams T, Blügel S, Rosch A, Mokrousov Y and Pfleiderer C 2014 *Phys. Rev. Lett.* **112** 186601
- [22] Huang S X and Chien C L 2012 *Phys. Rev. Lett.* **108** 267201
- [23] Schulz T, Ritz R, Bauer A, Halder M, Wagner M, Franz C, Pfleiderer C, Everschor K, Garst M and Rosch A 2012 *Nat. Phys.* **8** 301
- [24] Qin Q, Liu L, Lin W, Shu X, Xie Q, Lim Z, Li C, He S, Chow G M and Chen J 2019 *Adv. Mater.* **31** 1807008
- [25] Matsuno J, Ogawa N, Yasuda K, Kagawa F, Koshibae W, Nagaosa N, Tokura Y and Kawasaki M 2016 *Sci. Adv.* **2** e1600304
- [26] Kurumaji T, Nakajima T, Hirschberger M, Kikkawa A, Yamasaki Y, Sagayama H, Nakao H, Taguchi Y, Arima T and Tokura Y 2019 *Science* **365** 914
- [27] Kanazawa N, Nii Y, Zhang X X, Mishchenko A S, De Filippis G, Kagawa F, Iwasa Y, Nagaosa N and Tokura Y 2016 *Nat. Commun.* **7** 11622
- [28] Fujishiro Y, Kanazawa N, Nakajima T, Yu X Z, Ohishi K, Kawamura Y, Kakurai K, Arima T, Mitamura H, Miyake A, Akiba K, Tokunaga M, Matsuo A, Kindo K, Koretsune T, Arita R and Tokura Y 2019 *Nat. Commun.* **10** 1059
- [29] Göbel B, Akosa C A, Tatara G and Mertig I 2020 *Phys. Rev. Research* **2** 013315
- [30] Puphal P, Pomjakushin V, Kanazawa N, Ukleev V, Gawryluk D J, Ma J, Naamneh M, Plumb N C, Keller L, Cubitt R, Pomjakushina E and White J S 2020 *Phys. Rev. Lett.* **124** 017202
- [31] Vistoli L, Wang W, Sander A, Zhu Q, Casals B, Cicheler R, Barthélémy A, Fusil S, Herranz G, Valencia S, Abrudan R, Weschke E, Nakazawa K, Kohno H, Santamaria J, Wu W, Garcia V and Bibes M 2019 *Nat. Phys.* **15** 67
- [32] Hirschberger M, Nakajima T, Gao S, Peng L, Kikkawa A, Kurumaji T, Kriener M, Yamasaki Y, Sagayama H, Nakao H, Ohishi K, Kakurai K, Taguchi Y, Yu X, Arima T and Tokura Y 2019 *Nat. Commun.* **10** 5831
- [33] Khanh N D, Nakajima T, Yu X, Gao S, Shibata K, Hirschberger M, Yamasaki Y, Sagayama H, Nakao H, Peng L, Nakajima K, Takagi R, Arima T, Tokura Y and Seki S 2020 *Nat. Nanotechnol.* **15** 444
- [34] Mühlbauer S, Binz B, Jonietz F, Pfleiderer C, Rosch A, Neubauer A, Georgii R and Böni P 2009 *Science* **323** 915
- [35] Yu X Z, Kanazawa N, Onose Y, Kimoto K, Zhang W Z, Ishiwata S, Matsui Y and Tokura Y 2011 *Nat. Mater.* **10** 106
- [36] Yu X Z, Onose Y, Kanazawa N, Park J H, Han J H, Matsui Y, Nagaosa N and Tokura Y 2010 *Nature* **465**

- [37] Seki S, Yu X Z, Ishiwata S and Tokura Y 2012 *Science* **336** 198
- [38] Kézsmárki I, Bordács S, Milde P, Neuber E, Eng L M, White J S, Rønnow H M, Dewhurst C D, Mochizuki M, Yanai K, Nakamura H, Ehlers D, Tsurkan V and Loidl A 2015 *Nat. Mater.* **14** 1116
- [39] Tokunaga Y, Yu X Z, White J S, Rønnow H M, Morikawa D, Taguchi Y and Tokura Y 2015 *Nat. Commun.* **6** 7638
- [40] Seki S, Kim J H, Inosov D S, Georgii R, Keimer B, Ishiwata S and Tokura Y 2012 *Phys. Rev. B* **85** 220406(R)
- [41] Ghimire N J, Dally R L, Poudel L, Jones D C, Michel D, Magar N T, Bleuel M, McGuire M A, Jiang J S, Mitchell J F, Lynn J W and Mazin I I 2020 *Sci. Adv.* **6** eabe2680
- [42] Batista C D, Lin S Z, Hayami S and Kamiya Y 2016 *Rep. Prog. Phys.* **79** 084504
- [43] Li H, Ding B, Chen J, Li Z, Hou Z, Liu E, Zhang H, Xi X, Wu G and Wang W 2019 *Appl. Phys. Lett.* **114** 192408
- [44] Wang K, Mori R, Wang Z, Wang L, Ma J H S, Latzke D W, Graf D E, Denlinger J D, Campbell D, Bernevig B A, Lanzara A and Paglione J 2021 *npj Quantum Mater.* **6** 28
- [45] Nakamura A, Uejo T, Harima H, Araki S, Kobayashi T C, Nakashima M, Amako Y, Hedo M, Nakama T and Ōnuki Y 2016 *J. Alloys Compd.* **654** 290
- [46] Shang T, Xu Y, Gawryluk D J, Ma J Z, Shiroka T, Shi M and Pomjakushina E 2021 *Phys. Rev. B* **103** L020405
- [47] Araki S, Ikeda Y, Kobayashi T C, Nakamura A, Hiranaka Y, Hedo M, Nakama T and Ōnuki Y 2014 *J. Phys. Soc. Jpn.* **83** 015001
- [48] Nakamura A, Hiranaka Y, Hedo M, Nakama T, Miura Y, Tsutsumi H, Mori A, Ishida K, Mitamura K, Hirose Y, Sugiyama K, Honda F, Takeuchi T, Matsuda T D, Yamamoto E, Haga Y and Ōnuki Y 2014 *JPS Conf. Proc.* **3** 011012
- [49] Nakamura A, Uejo T, Honda F, Takeuchi T, Harima H, Yamamoto E, Haga Y, Matsubayashi K, Uwatoko Y, Hedo M, Nakama T and Ōnuki Y 2015 *J. Phys. Soc. Jpn.* **84** 124711
- [50] Shimomura S, Murao H, Tsutsui S, Nakao H, Nakamura A, Hedo M, Nakama T and Ōnuki Y 2019 *J. Phys. Soc. Jpn.* **88** 014602
- [51] Kobata M, Fujimori S, Takeda Y, Okane T, Saitoh Y, Kobayashi K, Yamagami H, Nakamura A, Hedo M, Nakama T and Ōnuki Y 2016 *J. Phys. Soc. Jpn.* **85** 094703
- [52] Nakamura A, Hiranaka Y, Hedo M, Nakama T, Miura Y, Tsutsumi H, Mori A, Ishida K, Mitamura K, Hirose Y, Sugiyama K, Honda F, Settai R, Takeuchi T, Hagiwara M, D Matsuda T, Yamamoto E, Haga Y, Matsubayashi K, Uwatoko Y, Harima H and Ōnuki Y 2013 *J. Phys. Soc. Jpn.* **82** 104703
- [53] Kneidinger F, Salamakha L, Bauer E, Zeiringer I, Rogl P, Blaas-Schenner C, Reith D and Podloucky R 2014 *Phys. Rev. B* **90** 024504
- [54] Ali M N, Xiong J, Flynn S, Tao J, Gibson Q D, Schoop L M, Liang T, Haldolaarachchige N, Hirschberger M, Ong N P and Cava R J 2014 *Nature* **514** 205
- [55] Liang T, Gibson Q, Ali M N, Liu M, Cava R J and Ong N P 2015 *Nat. Mater.* **14** 280
- [56] Wang Z, Weng H, Wu Q, Dai X and Fang Z 2013 *Phys. Rev. B* **88** 125427
- [57] Huang X, Zhao L, Long Y, Wang P, Chen D, Yang Z, Liang H, Xue M, Weng H, Fang Z, Dai X and Chen G 2015 *Phys. Rev. X* **5** 031023
- [58] Tafti F F, Gibson Q D, Kushwaha S K, Haldolaarachchige N and Cava R J 2016 *Nat. Phys.* **12** 272
- [59] Leahy I A, Lin Y P, Siegfried P E, Treglia A C, Song J C W, Nandkishore R M and Lee M 2018 *Proc. Natl. Acad. Sci. U.S.A.* **115** 10570 and the references therein
- [60] Nagaosa N, Sinova J, Onoda S, MacDonald A H and Ong N P 2010 *Rev. Mod. Phys.* **82** 1539
- [61] Tian Y, Ye L and Jin X 2009 *Phys. Rev. Lett.* **103** 087206
- [62] Hou D, Su G, Tian Y, Jin X, Yang S A and Niu Q 2015 *Phys. Rev. Lett.* **114** 217203
- [63] Yu X Z, Tokunaga Y, Kaneko Y, Zhang W Z, Kimoto K, Matsui Y, Taguchi Y and Tokura Y 2014 *Nat. Commun.* **5** 3198
- [64] Stavinoha M, Cooley J A, Minasian S G, McQueen T M, Kauzlarich S M, Huang C L and Morosan E 2018 *Phys. Rev. B* **97** 195146

Giant MR and THE in the EuGa₄ antiferromagnet

[65] In the momentum-space scenario, the ‘anomalous Hall effect’ is often used in the literature to denote any contribution other than the ordinary Hall effect. Here, we use the ‘topological Hall effect’ to denote the contribution in addition to the ordinary- and the *conventional* anomalous Hall effect. The topological Hall effect we discuss here is the topologically nontrivial part of the anomalous Hall effect.